The Development of Models for Carbon Dioxide Reduction Technologies for Spacecraft Air Revitalization

Michael J. Swickrath* and Molly Anderson†
NASA Johnson Space Center, Houston, TX, 77058

Through the respiration process, humans consume oxygen (O_2) while producing carbon dioxide (CO_2) and water (H_2O) as byproducts. For long term space exploration, CO_2 concentration in the atmosphere must be managed to prevent hypercapnia. Moreover, CO_2 can be used as a source of oxygen through chemical reduction serving to minimize the amount of oxygen required at launch. Reduction can be achieved through a number of techniques. NASA is currently exploring the Sabatier reaction, the Bosch reaction, and co-electrolysis of CO_2 and H_2O for this process. Proof-of-concept experiments and prototype units for all three processes have proven capable of returning useful commodities for space exploration.

All three techniques have demonstrated the capacity to reduce CO_2 in the laboratory, yet there is interest in understanding how all three techniques would perform at a system level within a spacecraft. Consequently, there is an impetus to develop predictive models for these processes that can be readily rescaled and integrated into larger system models. Such analysis tools provide the ability to evaluate each technique on a comparable basis with respect to processing rates. This manuscript describes the current models for the carbon dioxide reduction processes under parallel developmental efforts. Comparison to experimental data is provided were available for verification purposes.

Nomenclature

ASR	= Area specific resistance, [Ω-cm^2]
Btu	= British thermal unit
CH_4	= Methane
C(s)	= Solid carbon or coke
CO	= Carbon monoxide
CO_2	= Carbon dioxide
e^-	= Electron
H_2	= Diatomic hydrogen
H_2O	= Water
O_2	= Diatomic oxygen
N_2	= Diatomic nitrogen
PSIA	= Pounds per square inch (absolute)
rWGS	= Reverse water gas shift reaction
SLM	= Standard liters per minute

*Analyst, Crew and Thermal Systems Division, 2101 NASA Parkway, EC211, Houston, TX, 77058, AIAA Member.
†Analysis Lead, Crew and Thermal Systems Division, 2101 NASA Parkway, EC211, Houston, TX, 77058, AIAA Member.

I. Introduction

DURING space exploration, crew members consume food, which in turn is metabolized with oxygen (O_2), producing carbon dioxide (CO_2) and water (H_2O). Water can be purified and returned to the potable water storage tank. Alternatively, water can be electrolyzed and converted to oxygen and hydrogen (H_2). In addition, expired carbon dioxide can be reacted through a variety of techniques to produce additional water. The byproducts of further processing are either solid carbon (C(s)) waste or methane (CH_4) which can be either vented to space or used as a fuel source. A variety of these techniques under investigation for space exploration are summarized in fig. 1 and will be described in detail in the next few sections.

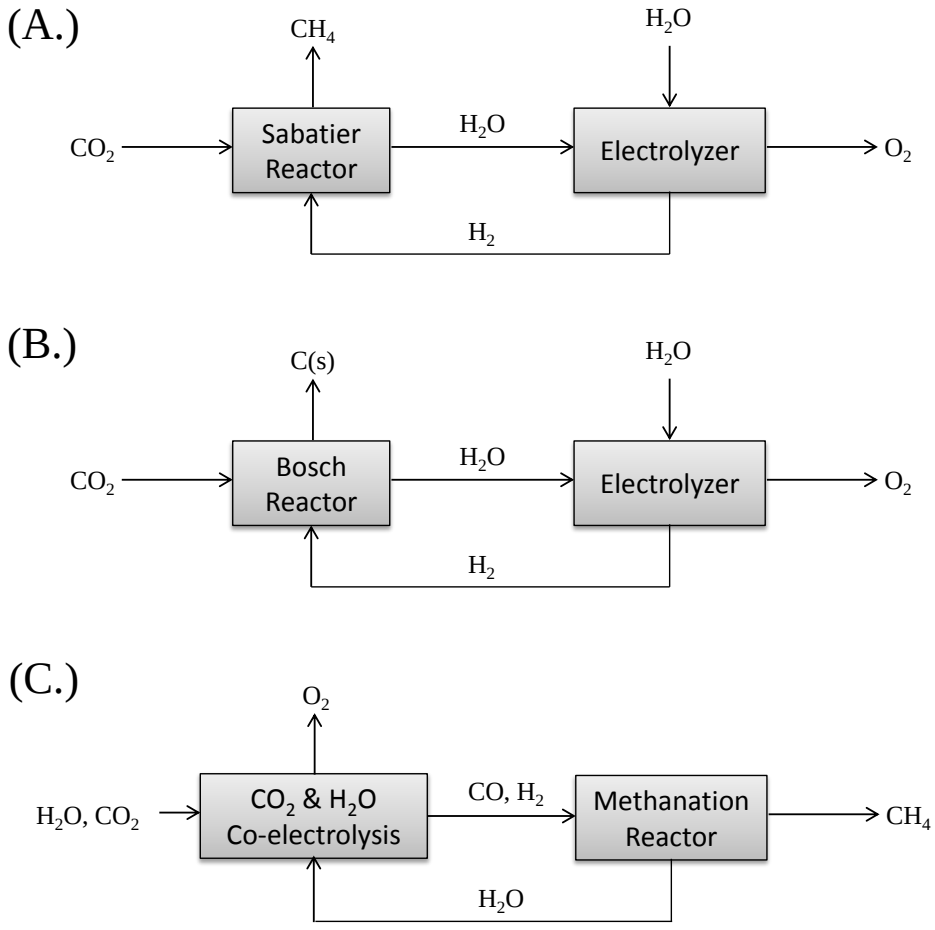

Figure 1: Flow diagrams for air revitalization techniques under consideration for space exploration. Specifics on each diagram are summarized elsewhere.[1] (A) The Sabatier reaction process. (B) The Bosch reaction process. (C) Carbon dioxide and water co-electrolysis and methanation.

A. Sabatier Process

The Sabatier reaction, also referred to as carbon dioxide methanation, involves reacting CO_2 and H_2 using iron, nickel, or ruthenium catalysts producing H_2O and CH_4 as described by eq. 1 and eq. 2 below.[2]

$$CO_2 + 4H_2 \rightleftharpoons CH_4 + 2H_2O \tag{1}$$

$$CO + 3H_2 \rightleftharpoons CH_4 + H_2O \tag{2}$$

The reaction is typically performed at temperatures ranging from 150°C (302°F) to 350°C (662°F) depending upon the catalyst.[3–5] The process is highly exothermic (ΔH = -165.4 kJ/mol) and therefore may require active cooling during reaction to prohibit temperature rising outside the favorable reaction zone. The advantage of the Sabatier reaction is that the lack of solid carbon formation leads to low reactor maintenance. The disadvantage includes the formation of CH_4 which would either be vented (associated with a loss in hydrogen commodities) or require downstream processing for either storage or combustion back to CO_2 and H_2O . It is also worth noting that the components involved in the Sabatier reaction can also undergo a reverse water-gas shift (rWGS) reaction which will be discussed in detail in the next few sections. However, for the temperatures involved in implementing the Sabatier reaction, the rWGS does not occur to any appreciable extent. While discussion on a Sabatier model is included within this manuscript, the breadth of the model verification efforts focus on the Bosch and co-electrolysis processes sincethe Sabatier models have been previously validated in other reports.[6–9]

B. Bosch Process

The Bosch process involves reacting CO_2 and H_2 to produce solid carbon and H_2O. The overall reaction completely closes the oxygen and hydrogen cycle and is represented below by equation 3.

$$CO_2 + 2H_2 \rightarrow C(s) + 2H_2O \tag{3}$$

The overall reaction is the sum of three separate reactions including the: reverse water-gas shift reaction (eq. 4), hydrogenation reaction (eq. 5), and Boudouard reaction (eq. 6).

$$CO_2 + H_2 \rightleftharpoons CO + H_2O \tag{4}$$

$$CO + H_2 \rightleftharpoons C(s) + H_2O \tag{5}$$

$$2CO \rightleftharpoons C(s) + CO_2 \tag{6}$$

The reaction is performed at high temperatures (approximately 650°C or 1202°F)in the presence of a catalyst (*e.g.* iron, cobalt, nickel, or ruthenium). The Bosch reactor system model was developed to simulate results from a system previously reported[10] since results exist that allow for model correlation and verification. The reactor system is fed with a mixture of H_2 and CO_2 at low temperature. The feed stream mixes with a recycle stream with gas that has been dried via a condensing heat exchanger. The mixed gas then passes through a heat exchanger that makes use of the enthalpy of the outlet gas to partially pre-heat the feed stream. The feed then enters the Bosch reactor first passing through a heater. After heating the gas to the reaction temperature, the gas enters the annular catalyst-packed Bosch reactor. The reactor exit gas passes back through the heat exchanger to pre-heat the feed stream before a portion is removed from a gas splitter.

The advantage of increased closure in the oxygen and hydrogen cycles comes at the expense of increased pressure drop and loss of catalyst activity due to coke formation as the reactor is used. For applications associated with space exploration, the Bosch reactor requires an increase in consumable mass for extra catalyst and an increase in crew time for reactor maintenance. As development efforts lead to advances in the Bosch reactor system, trade studies will need to be conducted to determine whether the increased catalyst consumables mass and crew time required for maintenance lowers oxygen and hydrogen launch mass enough to warrant implementation.

C. Co-electrolysis Process

Co-electrolysis is a combined process involving electrolysis of both H_2O and CO_2 as well as the reverse water-gas shift (rWGS) reaction (eq. 4) in solid oxide electrolysis cells.[1] The cell itself is essentially identical to a fuel cell operated in reverse. Specifically, power is introduced to the cell to facilitate a reaction rather than returned from the cell as a reaction proceeds. The cathode and anode side as well as the overall reactions are represented below by Eq. 7–9.

$$\text{Cathode: } xCO_2 + yH_2O + 4e^- \rightarrow xCO + yH_2 + 2O^- \tag{7}$$

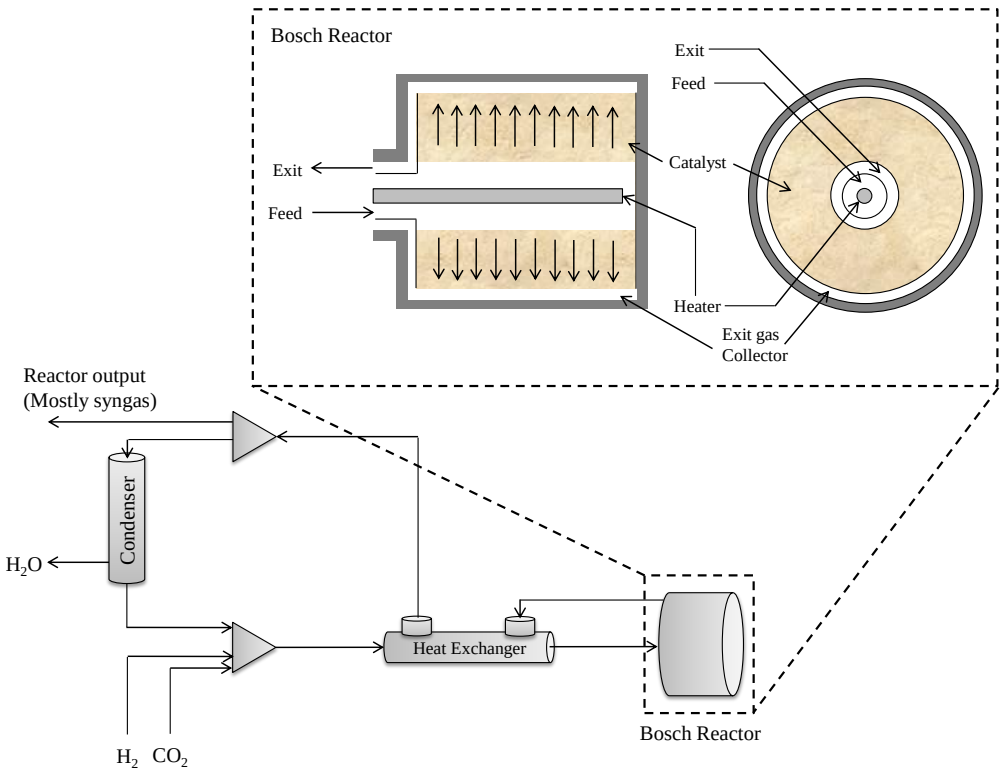

Figure 2: Bosch reaction system components and reactor diagram.

$$\text{Anode: } 2O^- \rightarrow O_2 + 4e^- \tag{8}$$

$$\text{Overall: } xCO_2 + yH_2O \rightarrow xCO + yH_2 + O_2 \tag{9}$$

The oxygen produced provides additional gas for metabolic respiration while CO and H_2 can be further processed through a Fischer-Tropsch reaction to produce hydrocarbon fuel sources.

The reaction occurs at relatively high temperatures of up to approximately 800°C.[1] For the reactor system, a heater in front of the electrolysis cell stack preheats the inlet gas to the appropriate temperature. The inlet gas is then introduced to the porous cathode material (*e.g.* nickel-zirconia cermet) while an oxygen source is introduced to the porous anode side (*e.g.* strontium-doped lanthanum manganite). The voltage supplied from the anode to cathode side facilitates the co-electrolysis process.

The area specific resistance (ASR) of the cell stack influences the degree of conversion achieved. The ASR is dependent upon the materials and methods used to fabricate the cell, the fidelity of the manufacturing process, the feed-stock composition, and the operating temperature. Laboratory data collected for a feedstock of humid air and humid air with CO_2 show nearly identical ASR values as a function of stack current. Alternatively, for a feedstock of dry CO_2, a much higher ASR value is achieved.[11] This result seems to suggest that H_2O is consumed in the electrochemical reaction within the cell while CO_2 is then consumed through the rWGS reaction as H_2O electrolysis shifts compositions away from the equilibrium composition for a given operating temperature.

The advantage of the co-electrolysis process is that it avoids solid carbon formation. Moreover, in comparison to the Bosch reactor system, the co-electrolysis process reduces the number of components required for CO_2 reduction. Furthermore, it allows for water electrolysis in vapor phase eliminating two-phase flow problems that can occur in a low-gravity environment associated with alternative H_2O electrolysis technologies. Current challenges toward applying this technology for space exploration pertain mostly to cell degradation over time and issue associated with manufacturability that are still under investigation.[1,12]

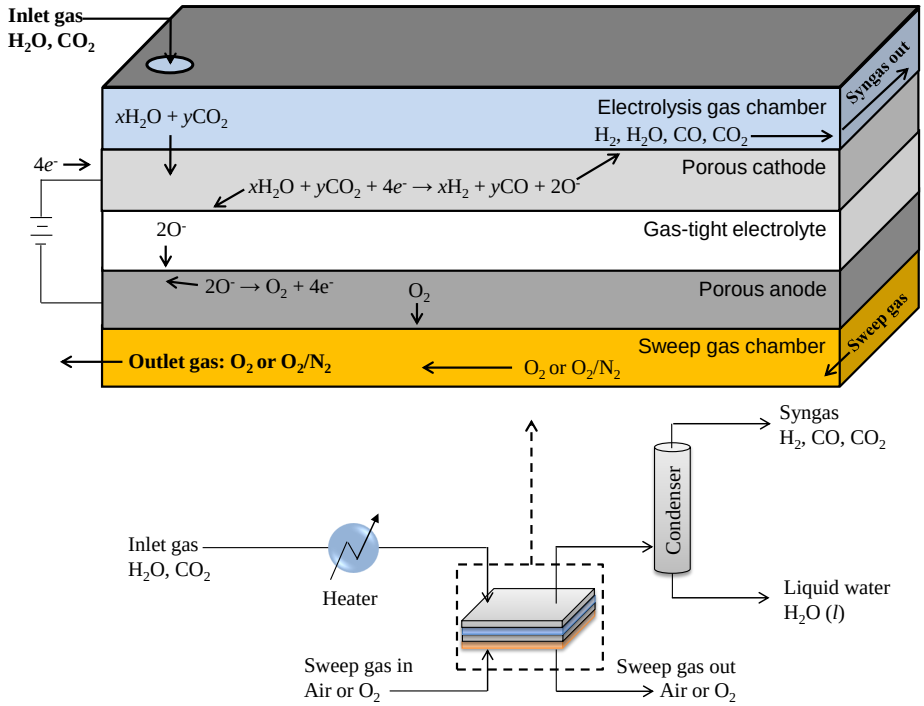

Figure 3: Co-electrolysis reaction system components and reaction occurring within the solid oxide electrolysis cell.

II. Carbon Dioxide Reduction Modeling & Simulation

For each reaction process previously described, proof-of-concept experiments and lab-scale prototypes have demonstrated their capability to effectively reduce CO_2 producing other useful gas commodities (*e.g.* H_2O, H_2, O_2, CH_4). However, a direct comparison of the laboratory results to evaluate each technology is not readily possible for a variety of reason. For example, laboratory prototypes are of various processing scales leading to uncertainty with respect to how to compare results for these technologies on a consistent basis. Due to cost/schedule constraints, the entire parameter space (*e.g.* reaction temperature/pressure, composition, recycle ratio) for each technology might not have been exhaustively bounded. Furthermore, most experimental units have been evaluated in stand-alone test configurations rather than as part of a larger system. This eliminates any coupling effects that may exist within an integrated subsystem.

Consequently, there is an impetus towards developing first principles models for each technology. The development of such models will allow for the investigation of a wide parameter space, contingency mode operations otherwise dangerous or expensive to perform in the laboratory, and to assess in-system performance when perturbations can be introduced either deterministically or stochastically to boundary conditions. This manuscript discusses‘ the first principles models established in fiscal year 2011 for each process using the experimental results in the literature as validation.

A. Representation of Reaction Rate Expressions

Kinetic models were established for each individual carbon dioxide reduction technology. Because some of the elementary reaction mechanisms were similar between some of the reactors, the models were deliberately constructed to maintain flexibility so that reaction steps and intermediate components could easily be added or removed for each system. This was achieved using the formalism established by Rawlings and Ekertd[13] and Fogler.[14] For the species list denoted by the string-vector A (and A^T as A transposed), and the stoichiometric

matrix ν, the complete system of reactions defined in the preceding sections can be represented as in eq. 10.

$$\nu A = 0 \tag{10}$$

$$A^T = \begin{bmatrix} \text{C(s)} & \text{CO} & \text{CO}_2 & \text{CH}_4 & \text{H}_2 & \text{H}_2\text{O} \end{bmatrix} \tag{11}$$

$$\nu = \begin{bmatrix} 0 & 0 & -1 & 1 & -4 & 2 \\ 0 & -1 & 0 & 1 & -3 & 1 \\ 0 & 1 & -1 & 0 & -1 & 1 \\ 1 & -1 & 0 & 0 & -1 & 1 \\ 1 & -2 & 1 & 0 & 0 & 0 \\ 0 & 1 & -1 & 0 & 0 & 0 \\ 0 & 0 & 0 & 0 & 1 & -1 \end{bmatrix} \tag{12}$$

The rows of matrix ν are associated with the following reactions in order: (1) methanation of CO_2, (2) methanation of CO, (3) the reverse water gas shift reaction, (4) the hydrogenation reaction, (5) the Boudouard reaction, (6) CO_2 electrolysis and (7) H_2O electrolysis. Each separate reaction i (for $i \in [1, 7]$) has an associated reaction rate r_i, which in aggregate compose the reaction rate vector r. Each species j (represented in A), has an associated species production rate for reaction i, denoted as $R_{i,j}$, representing matrix R. For vector M representing the molecular weights of vector A, the conservation of mass can be posed as $\nu M = 0$. Furthermore, the relationship between reaction rate and species production rate is $R = \nu^T r$. To simulate a specific reaction process, rows of the r vector can be turned 'on' or 'off' by multiplication by 1 or 0 (*e.g.* the Bosch reaction process is enabled if rows 1, 2, 6, and 7 are multiplied by 0 and rows 3-5 are multiplied by 1). In this manner, a general model can be constructed that can easily be adapted to a Bosch or Sabatier reaction. Alternatively, adaptation to co-electrolysis requires modification to momentum balance.

B. Bosch and Sabatier Momentum and Energy Balances

For the Bosch and Sabatier systems, the reactor modeled was similar to the annular system of Bunnell, et al.[10] (see: fig. 2). The species transport equation, neglecting dispersion, is formulated below in tensor notation.

$$\frac{\partial C_j}{\partial t} = \nabla \cdot (\vec{v} C_j) + \sum_i \nu_{i,j} r_i \tag{13}$$

As previously discussed, j denotes species, i represents all possible reactions (*e.g.* methanation, hydrogenation, rWGS, Boudouard), and $\vec{v}$ is the interstitial velocity vector. Eq. 13 is reduced to a one-dimensional form under the assumption concentration and velocity gradients in the axial and angular directions are negligible.

$$\frac{\partial C_j}{\partial t} = \frac{1}{r} \frac{\partial (r v_r C_j)}{\partial r} + \sum_i \nu_{i,j} r_i \tag{14}$$

From this point forward, radial interstitial velocity v_r will simply be denoted as v. Moreover, rvC_j represents convective flux of species j. The spatial derivative of this term can be computed via the chain rule. However, to improve the stability of the numerical model and avoid having to carry additional differential terms, a new variable is introduced in the numerical model for species convective flux $\phi_j = rvC_j$.

$$\frac{\partial C_j}{\partial t} = \frac{1}{r} \frac{\partial (\phi_j)}{\partial r} + \sum_i \nu_{i,j} r_i \tag{15}$$

Velocity is related to volumetric flow rate $\dot{V}$, through reactor cross-sectional area ($2\pi rL$) according to $\dot{V} = 2\pi rLv$. During reaction, moles reacted and moles produced are not commensurate. Furthermore, as phase change occurs during coke formation, moles are accumulated within the reactor. Consequently, volumetric flow rate will not be constant and needs to be accounted for appropriately. This is accounted for via the following proportionality.[14] Subscripts o denote inlet conditions and Z represents the compressibility

factor defined as the ratio of the molar density of the gas as if it behaved as an ideal mixture by the actual molar density of the gas.

$$\dot{V} = \dot{V}_o \left[\frac{P_o}{P} \frac{T}{T_o} \frac{Z}{Z_o} \right] \tag{16}$$

The void fraction, ϵ, of the reactor changes with the formation of solid carbon (species 1) where ρ denotes the density of carbon (2250 kg/m^3). This in turn, influences the pressure-flow characteristics of the reactor according to Darcy's law.

$$\frac{\partial \epsilon}{\partial t} = \frac{1}{\rho_1} \frac{\partial C_1}{\partial t} \tag{17}$$

$$\frac{-\kappa}{\mu} \frac{\partial P}{\partial r} = v \tag{18}$$

In eq. 18, P denotes the total interstitial pressure in the reactor, κ is the Darcy permeability, and μ is the dynamic viscosity of the gas mixture. The Darcy permeability is a function of void fraction.[10] This dependency has been regressed in other studies.[15] The Darcy permeability is a function of total reactor solid carbon mass m_1, which arises from integrating local solid carbon concentrations over the reactor volume V.

$$m_1 = \frac{M_1}{V} \int_V C_1 dV \tag{19}$$

$$\kappa(\epsilon) = \begin{cases} \log \kappa = -9.2876 & \text{for } m_1 < 360.6 \text{ kg/m}^3 \\ \log \kappa = -0.001854 m_1 - 8.6190 & \text{for } m_1 \geq 360.6 \text{ kg/m}^3 \end{cases} \tag{20}$$

The momentum transport equations must also be solved simultaneously with an energy balance. Specifically, thermal gradients cause pressure gradients which can influence pressure-flow characteristics. Moreover, the reaction kinetics are highly sensitive to reactor temperature. Consequently, accurately accounting for thermal variations along the radial direction is imperative. The following energy balance was applied.

$$\rho C_p \frac{\partial T}{\partial t} = \sum_i \nu_{i,j} H_j r_i + h_r A_c (T_r - T) + Q \tag{21}$$

In eq. 21, ρ is the density of the interstitial gas, C_p is the constant pressure specific heat of the gas phase, H_j is the enthalpy of component j at the provided temperature, h_r is the convective heat transfer coefficient for the reactor, A_c is the specific area of the catalyst particles, T_r is the reactor set point temperature that is presumably the temperature at the reactor wall, and Q is the external heating/cooling rate. The second term of eq. 21 is heat generation/consumption due to reaction while the third term is associated with heat loss to the reactor wall.

C. Calculation of Equilibrium Coefficients

The reactions comprising the methanation, hydrogenation, rWGS, and Boudouard reactions are all equilibrium processes. Consequently, the relative deviation in composition from equilibrium determines the extent to which the reaction will occur. This also influences the reaction kinetics which are concentration dependent. For the general reaction equation represented below, an equilibrium constant can then be formulated, *viz.*

$$\alpha A + \beta B \rightleftharpoons \gamma C + \delta D \tag{22}$$

$$K_a = \prod_j [X_j]^{\nu_j} = \frac{[C]^\gamma [D]^\delta}{[A]^\alpha [B]^\beta} \tag{23}$$

In expression 23, the subscript a denotes the equilibrium coefficient is posed on the basis of component activity. The subsequent derivation of the rigorous calculation of the equilibrium coefficient follows the work of Sandler.[16] Activity is defined according to a ratio of component fugacity at actual conditions $f_j(T, P, z)$,

to the fugacity at reference conditions $f_j^\circ(T_\circ, P_\circ, z_\circ)$, and is related to a difference in Gibbs free energy of actual versus reference conditions.

$$a = \frac{f_j(T,P,z)}{f_j^\circ(T_\circ,P_\circ,z_\circ)} = \exp\left[\frac{G_j(T,P,z) - G_j^\circ(T_\circ,P_\circ,z_\circ)}{RT}\right] \tag{24}$$

From the definition of activity, the equilibrium coefficient expressed in activity can be recast according to the previous relationship.

$$\ln K_a = \ln \prod_{j=1}^{n} a_j^{\nu_j} = -\frac{\Delta G_{\text{rxn}}^\circ}{RT} \tag{25}$$

In order to capture the deviation in the equilibrium coefficient at temperatures excursions far from standard state, the van't Hoff equation is used.

$$\frac{d\ln K_a}{dT} = -\frac{1}{R}\frac{d}{dT}\left[\frac{\sum_j \nu_j \Delta G_{f,j}^\circ}{T}\right] = \frac{1}{RT^2}\sum_j \nu_j \Delta H_{f,j}^\circ = \frac{\Delta H_{\text{rxn}}^\circ(T)}{RT^2} \tag{26}$$

The change in the heat of reaction at elevated temperatures $\Delta H_{\text{rxn}}^\circ(T)$, which depends on the change in the mixture heat capacity ΔC_p, is calculated as follows.

$$\Delta H_{\text{rxn}}^\circ(T) = \Delta H_{\text{rxn}}^\circ(T_\circ) + \int_{T_\circ}^{T} \Delta C_p(T')dT' \tag{27}$$

The component heat capacities calculated from polynomial fits with data tabulated elsewhere.[17] The polynomial fits are provided from a series of coefficients (a_j through e_j) with the relationship ΔC_p according to reaction stoichiometry.

$$C_{p,j}(T) = a_j + b_j T + c_j T^2 + d_j T^3 + e_j T^{-2} \tag{28}$$

$$\begin{aligned}\Delta C_p &= \sum_j \nu_j a_j + \sum_j \nu_j b_j T + \sum_j \nu_j c_j T^2 + \sum_j \nu_j d_j T^3 + \sum_j \nu_j e_j T^{-2} \\ &= \Delta a + \Delta b T + \Delta c T^2 + \Delta d T^3 + \Delta e T^{-2}\end{aligned} \tag{29}$$

Equation 27 can then be integrated to provide the analytical relationship for heat of reaction at elevated temperatures.

$$\begin{aligned}\Delta H_{\text{rxn}}^\circ(T) = \Delta H_{\text{rxn}}^\circ(T_1) &+ \Delta a\,(T - T_1) + \frac{\Delta b}{2}\left(T^2 - T_1^2\right) \\ &+ \frac{\Delta c}{3}\left(T^3 - T_1^3\right) + \frac{\Delta d}{4}\left(T^4 - T_1^4\right) - \Delta e\left(T^{-1} - T_1^{-1}\right)\end{aligned} \tag{30}$$

Lastly, expression 30 is used with the van't Hoff equation (expression 26) with a subsequent integration to provide the temperature and composition dependency on the activity-based equilibrium coefficient, K_a.

$$\begin{aligned}\ln\frac{K_a(T_2)}{K_a(T_1)} = \frac{\Delta a}{R}\ln\frac{T_2}{T_1} &+ \frac{\Delta b}{2R}(T_2 - T_1) + \frac{\Delta c}{6R}\left(T_2^2 - T_1^2\right) + \frac{\Delta d}{12R}\left(T_2^3 - T_1^3\right) + \frac{\Delta e}{2R}\left(T_2^{-2} - T_1^{-2}\right) \\ &+ \frac{1}{R}\left[-\Delta H_{\text{rxn}}^\circ + \Delta a T_1 + \frac{\Delta b}{2}T_1^2 + \frac{\Delta c}{3}T_1^3 + \frac{\Delta d}{4}T_1^4 - \frac{\Delta e}{T_1}\right] \times \left[\frac{1}{T_2} - \frac{1}{T_1}\right]\end{aligned} \tag{31}$$

The pressure dependency is captured by employing 25 with the definition of activity, $a_j = z_j P/P_\circ$.

$$K_a = \prod_{j=1}^{n} a_j^{\nu_j} = \prod_{j=1}^{n}\left(z_j \frac{P}{P_\circ}\right)^{\nu_j} \tag{32}$$

The above derivation captures the temperature dependence of the equilibrium coefficient. Sometimes this is also modeled empirically. A great deal of work has been done to summarize this relationship for the rWGS reaction (reviewed in detail elsewhere[18]). Data for the rWGS and hydrogenation reactions have been tabulated in previous reports.[15] For the remaining reactions, equilibrium coefficients were calculated from first principles and a resulting relationship for the value of the coefficient as a function of temperature was developed using the following form.

$$K_i = \exp\left[\frac{\lambda_1}{T^2} + \frac{\lambda_2}{T} + \lambda_3\right] \tag{33}$$

The final relationships captured by equation 33 are much more straightforward to implement numerically rather than solving Eq. 29–31. For this analysis, both the rigorous derivation and fit to the resulting relationship were applied and show good agreement with one another. The models developed seemed to run with greater stability when equations in the form of 33 were used or when Eq. 29–31 were solved outside of the simulation using Fortran subroutines. In both cases, the results were compared to the existing data from previous reports[15] to confirm the approach was accurate.

The values associated with Table 1 are summarized herein. It is useful to look at the relationship as function of temperature. For a reaction to favor proceeding to any measurable degree, the equilibrium coefficient would need to exceed unity. Fig. 4A&B demonstrates the magnitude of the coefficients with respect to temperature. For the Sabatier reaction relying on CO_2 methanation, it is clearly evident that temperature should not exceed 600°C (1112°F) and should be operated at lower temperatures to drive equilibrium toward products. However, there is a balance to maintain with temperature for CO_2 methanation since the reaction rate is directly proportional to temperature. This is why the reaction is typically operated in the 150-300°C (302-572°F) range. Conversely, the rWGS and hydrogenation reactions involved in the Bosch and co-electrolysis process require high temperatures to drive the equilibrium to favor products. Moreover, at the temperatures amenable to rWGS and hydrogenation, the Boudouard reaction favors reactants which will provide CO to support additional hydrogenation. Lastly, it is worth noting that the slope of the $\ln K_a$ as a function of $1/T$ for the rWGS is negative whereas the rest of the reactions show a positive slope. This is manifest as the rWGS is endothermic ($\Delta H^\circ_{\text{rxn}}(T) > 0$) while all other reactions are exothermic. In other words, the rWGS requires energy to facilitate the reaction and to offset cooling as the reaction tends to completion; conversely, the other reactions require a certain amount of energy to promote the reaction and could need additional cooling to maintain the optimal reaction temperature. The trade between endothermal and exothermal effects will have implications on heating/cooling for the competing reactor systems.

Table 1: Equilibrium coefficient temperature dependency constants associated with eq. 33.

Description	Reaction	Equation	λ_1	λ_2	λ_3
1. CO_2 Methanation	$CO_2 + 4H_2 \rightleftharpoons CH_4 + 2H_2O$	Eq. 1	-730,726.0	24,125.3	-26.9616
2. CO Methanation	$CO + 3H_2 \rightleftharpoons CH_4 + H_2O$	Eq. 2	-538,798.1	28,062.7	-30.7759
3. Reverse WGS	$CO_2 + H_2 \rightleftharpoons CO + H_2O$	Eq. 4	-191,928.1	-3,937.4	3.8143
4. Hydrogenation	$CO + H_2 \rightleftharpoons C(s) + H_2O$	Eq. 5	-121,003.4	16,573.0	-17.3858
5. Boudouard	$2CO \rightleftharpoons C(s) + CO_2$	Eq. 6	70,924.7	20,510.4	-21.2000

D. Gas–Phase Equilibria Reaction Kinetics

The rate through which each reaction occurs is dependent upon feed composition, the reactor pressure, the catalyst material, and the reaction temperature. Consequently, the exact expected rate tends to be very dependent upon the designed application of the reactor system. In contrast, the models developed and described in this report are intended to be flexible and can be tailored toward reactor system undergoing iterative design and optimization. As a result, general rate expressions are discussed below while rate coefficients are provided for specific implementations of each reaction. Moving forward, the rate expressions are most likely generally applicable having been derived mechanistically from first principles. In contrast,

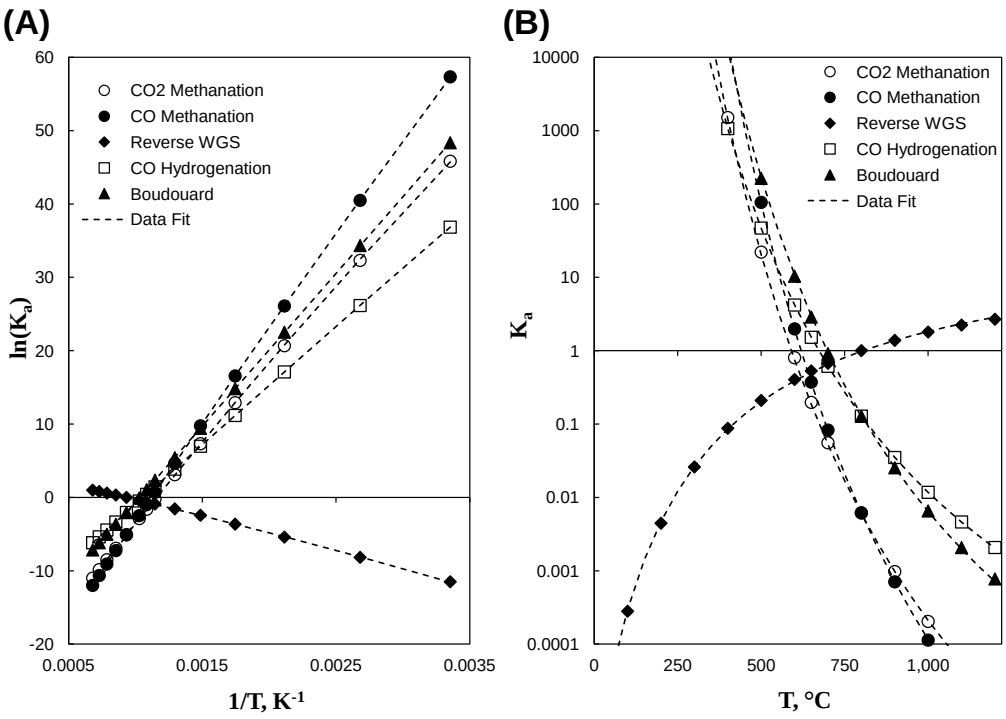

Figure 4: Equilibrium coefficients for reactions 1-5 along with the fit to each data set. (A) Linear fit to first principles calculation. (B) Trend of equilibrium coefficient K with temperature.

rate coefficients will most likely need adjustment with laboratory data as advances are made in the catalysts facilitating these reactions.

1. Carbon dioxide methanation

For the Sabatier reaction, studies for carbon dioxide methanation with commercial Ni/Al_2O_3 catalysts at 225-300°C (437-572°F), with 1-3 atm pressure, and H_2/CO_2 ratios of 4-5, have yielded the following rate expression where subscripts denote the row associated with each reaction in the matrix ν.[3,19]

$$r_1 = \frac{k_1 K_{CO_2,1} K_{H_2,1}^4 z_{CO_2} z_{H_2}^4 P^5}{\left(1 + K_{CO_2,1} P z_{CO_2} + K_{H_2,1} P z_{H_2}\right)^5} (1 - \eta) \tag{34}$$

In the above expression, z_j is associated with the mole fraction of species j and η is referred to as the approach to equilibrium. For the CO_2 methanation reaction, η is expressed as follows.

$$\eta = \frac{1}{K_1 P^2} \frac{z_{CH_4} z_{H_2O}^2}{z_{CO_2} z_{H_2}^4} \tag{35}$$

The rate constant k, and the other reaction constants are expressed as follows.

$$k_1[\text{mol/g-s}] = 1.064 \times 10^{11} \exp\left[\frac{-113,497.4}{R_g T}\right] \tag{36}$$

$$K_{CO_2,1}[\text{atm}^{-1}] = 9.099 \times 10^{-7} \exp\left[\frac{69,691.8}{R_g T}\right] \tag{37}$$

$$K_{H_2,1}[\text{atm}^{-1}] = 9.6104 \times 10^{-4} \exp\left[\frac{39,942.0}{R_g T}\right] \tag{38}$$

2. Reverse Water–Gas Shift & Hydrogenation

The reverse water–gas shift reaction (rWGS) and hydrogenation reactions were modeled according to previous studies.[15] The relationships are summarized below.

$$r_3 = k_3 \rho P \left(z_{CO_2} z_{H_2} K_3 - z_{CO} z_{H_2O} \right) \tag{39}$$

$$r_4 = k_4 \rho \left(z_{CO} z_{H_2} K_4 P - z_{H_2O} \right) \tag{40}$$

The rate constants for these expressions follow Arrhenius relationships. These expressions are listed below.

$$k_3[\text{1/bar-hr}] = 1.610 \times 10^9 \exp\left[\frac{-108,000}{R_g T}\right] \tag{41}$$

$$k_4[\text{1/bar-hr}] = 1.490 \times 10^7 \exp\left[\frac{-42,300}{R_g T}\right] \tag{42}$$

3. Boudouard Reaction

A detailed reaction rate model derived from first principles was employed for the Boudouard reaction in the presence of nickel carbide. The resulting model, derived elsewhere,[20] is listed below.

$$r_5 = \frac{\rho_{\text{cat}} \epsilon_o k_B^+ K_{CO,5} \left(P z_{CO} - \frac{1}{K_B^*} \frac{z_{CO_2}}{z_{CO}} \right)}{\left(1 + K_{CO,5} P z_{CO} + \frac{1}{K_{O,CO_2} K_{CO,5}} \frac{z_{CO_2}}{z_{CO}} \right)^2} \tag{43}$$

In eq. 43, ρ_{cat} represents the catalyst density (14,900 kg/m^3 for nickel carbide or 7,850 kg/m^3 for carbon steel), ϵ_o represents the density the void fraction of the catalyst prior to coke formation, K_B^* is the coking threshold where gasification and carbon formation rates are equivalent, k_B^+ is the net forward reaction rate of the rate determining step, and K_{O,CO_2} and $K_{CO,5}$ are equilibrium coefficients for intermediate steps of the proposed reaction mechanism by Snoeck et al.[20] The expression of the rate constants and equilibrium coefficients are as follows.

$$k_B^+ = 26.733 \times 10^7 \exp\left[\frac{-108,379}{R_g T}\right] \tag{44}$$

$$K_B^* = \exp\left[\frac{162,483}{R_g T} - 20.499\right] \tag{45}$$

Formulas were not provided for the coefficients K_{O,CO_2} and $K_{CO,5}$ by Snoeck et al. In lieu of formulas, expected ranges were supplied instead for these parameters. Since the ranges were relatively narrow, an average of the maximum and minimum values were utilized in the model ($K_{O,CO_2} = 41.3$ bar and $K_{CO,5} = 0.113$ bar^{-1}).

E. Gas Co-electrolysis Kinetics

The co-electrolysis reaction is performed in phases. First, the gas flows through a segment of heated catalyst where the rWGS reaction occurs according to previously discussed relationship (see: eq. 39 and eq. 41). Following the heating stage, co-electrolysis is performed to crack the water to oxygen and hydrogen gas. The produced hydrogen gas serves to further drive the equilibrium of the rWGS reaction toward the production of CO and H_2O as would be expected from Le Chatelier's principle. To model this process, an additional generation/consumption term is added to the material balance representing the rate of monatomic oxygen removal in the cell, ΔN_O.

$$\Delta N_O = \frac{i_c n_c A_c}{2F \left(N_{CO_2} + N_{H_2O} \right)} \tag{46}$$

In eq. 46, i_c is the current to each cell, A_c represents the area of a single cell, n_c is the number of cells in the co-electrolysis stack, F is Faraday's constant, and N_j is the total molar flow rate of component j with j

representing the sources of monatomic oxygen (CO_2 or H_2O). In the co-electrolysis process, CO_2 and H_2O are consumed producing CO and H_2. The numerator in eq. 46 is the total ionic current to the co-electrolysis cell stack which will be referred to as I_e for the remainder of this report.

Co-electrolysis cells are small and residence times are short. As a result, for model construction, cells were idealized to a continuous-stirred tank reactor type of a model.

$$\frac{\partial n_j}{\partial t} = z_j N - z_{j,o} N_o + \nu_{3,j} r_3 + \sum_{i=6}^{7} \nu_{i,j} r_i \tag{47}$$

Mole fractions of component j are represented by z_j, molar flow rates are represented by N, n_j represents instantaneous moles of component j in the electrolysis cell, and r_3 is the rWGS reaction. A subscript o denotes the value of a parameter at the inlet of the cell. The first term represents the accumulation/generation of components in the electrolysis cell. The second and third terms are component flow into and out of the cell, respectively. The fourth term represents the rWGS reaction. The final term in eq. 47 is associated with the co-electrolysis process which was modeled as independent CO_2 and H_2O electrolysis steps.[21]

$$CO_2 + 2e^- \rightarrow CO + O^{2-} \tag{48}$$

$$H_2O + 2e^- \rightarrow H_2 + O^{2-} \tag{49}$$

Reaction rates for co-electrolysis arise from the rate of monatomic oxygen removal. Components in the cell are assumed to be dispersed evenly, and as a result, oxygen produced from CO_2 and from H_2O is presumably proportional to the fraction of CO_2 or H_2O present in the cell.

$$r_6 = \Delta N_O \left[\frac{z_{CO_2}}{z_{CO_2} + z_{H_2O}} \right] \tag{50}$$

$$r_7 = \Delta N_O \left[\frac{z_{H_2O}}{z_{CO_2} + z_{H_2O}} \right] \tag{51}$$

The energy equation for the co-electrolysis process is formulated as follows based on the efforts reported in previous analyses.[1]

$$Q - W = N \sum_j z_j \left(\Delta H^o_{f,j} + H_j(T) - H^o_j \right) - N_o \sum_j z_{j,o} \left(\Delta H^o_{f,j} + H_j(T_o) - H^o_j \right) \tag{52}$$

The term Q is the external heat transfer rate to or from the electrolyzer, W is the rate of electrical work, $\Delta H^o_{f,j}$ is the standard-state enthalpy of formation, and $H_j(T) - H^o_j$ is the sensible enthalpy. Electrical work is proportional to the operating voltage V_{op}, and the total ionic current $W = V_{op} I_e$. However, the operating voltage is the sum of mean Nernst potential of the cell V_N, associated with electrochemical reaction and the loss of potential through inefficiencies intrinsic to the cell and quantified by a term referred to as the area specific resistance, ASR.

$$V_{op} = V_N + i_c \mathrm{ASR} \tag{53}$$

The mean Nernst operating potential of the cell depends on the temperature and composition gradients across the cell and was calculated on the basis of water (although an equivalent value can be calculated from the basis of carbon dioxide).

$$V_N = \frac{1}{\xi} \int_{T_o}^{T} \int_{z_{O_2,o}}^{z_{O_2}} \int_{z_{H_2,o}}^{z_{H_2(T)}} \Delta G_{R,H_2O} + R_g T \ln \left[\frac{z_{H_2O}}{z_{H_2} z_{O_2}^{1/2}} \right] dz_{H_2} dz_{O_2} dT \tag{54}$$

$$\xi = 2F \left(T - T_o \right) \left(z_{O_2} - z_{O_{2,o}} \right) \left(z_{H_2}(T) - z_{H_{2,o}} \right) \tag{55}$$

In eq. 55, $\Delta G_{R,H_2O}$ is the Gibbs free energy change associated with water hydrolysis at the elevated reactor temperature. The calculation of $\Delta G_{R,j}$ for non-ideal conditions is fairly involved and is explained in detail by Sandler.[16] Because the integral bounds are temperature dependent, then either an outlet temperature or an external heat transfer rate must be specified in order to arrive at a solution through solving equations 52

and 54 simultaneously. Once specified, the outlet composition and power requirements can be determined for the co-electrolysis cell stack. The solution to this integral will be discuss in further detail in latter sections of this report.

III. Results and Verification

Models for the carbon dioxide reduction techniques discussed herein have been generated in the Aspen Custom Modeler® software package (Aspen Technology Inc., Burlington, MA). The calculations were performed on a central processing unit (CPU) with a 2.66 GHz Intel® Core™2 Quad processor (Intel Corporation, Santa Clara, CA) and 3.25 GB of random access memory (RAM).

A. Bosch Modeling Results

The Bosch reactor system was generated as an analog to the reactor system developed by Bunnell et al.[10] As the reaction proceeds, solid carbon is formed upon the catalyst through the hydrogenation and Boudouard reactions. The formation of solid carbon, or coke, is problematic as it decreases the void fraction within the reactor increasing pressure drop. Moreover, as carbon forms, it begins coating the catalyst material interfering with the activity of the catalyst. For this analysis, the relationship between the carbon density within the reactor and the pressure drop are of critical importance for reactor and system performance.

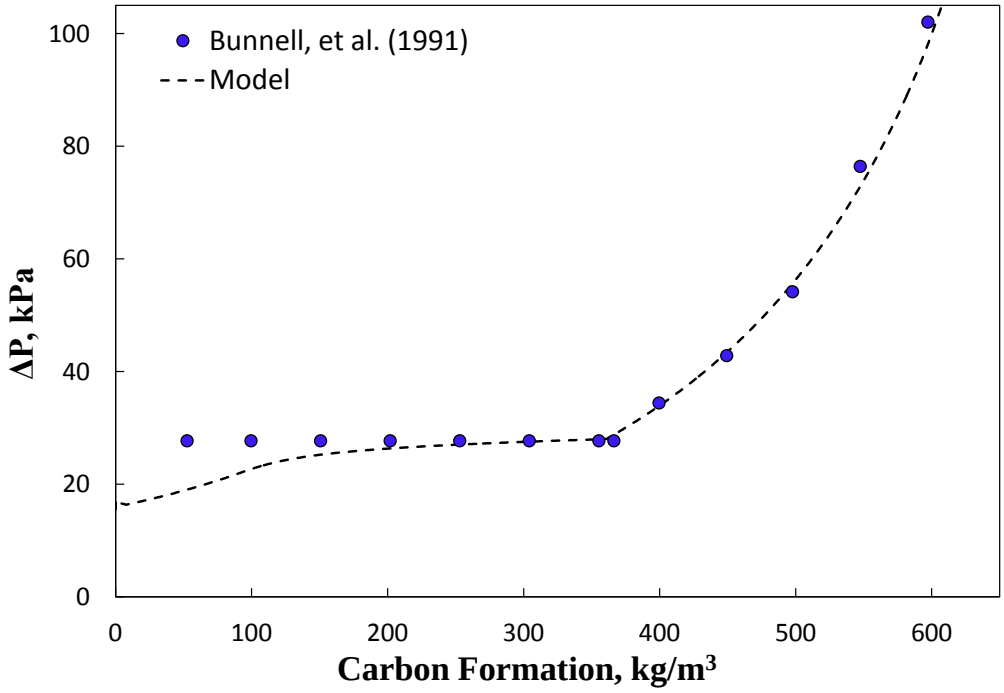

Figure 5: Pressure drop as a function of solid carbon formation within the Bosch reactor in comparison to results collected by Bunnell et al.[10] The processing rate is equivalent to a crew of four personnel.

Fig. 5 demonstrates the relationship between pressure drop and carbon formation. The processing rate was established to mimic the requirements for a crew of four personnel. The results between the model and Bunnell et al.[10] are in good agreement. As the reaction proceeds, coke is formed. At the inner radius of the annular reactor, the void fraction changes fairly rapidly with coke formation. As the radius is increased, the differential volume between r and $r + \Delta r$ scales to the second-order. Consequently, so long as the reactor temperature and feed composition are relatively constant, an increase in radius is accompanied with a pronounced decrease in the dynamics at which the void fraction changes. As indicated in fig. 5, the pressure drop is fairly constant until a density of approximately 370 kg/m^3 is reached. After this threshold is met, the

pressure drop increases precipitously with additional coke formation. The dynamics of this process are on the order of 100s of hours depending on the processing rate and recycle ratio. Although reactor dimensions have not been parametrically explored at the time of compiling this report, these results allude to the importance of the optimizing reactor geometry for provided processing requirements.

As of the end of fiscal year 2011, the Bosch model is operational and is returning results. Individual components of the system model are running with good stability. However, the overall numerical stability of the system as a whole stands to be improved. Future efforts will focus on improving the model stability as well as performing parametric analyses exploring predicted system performance. Furthermore, larger system models for vehicle air revitalization may make use of the Bosch/Sabatier reactor model as a means to explore their in-system performance in comparison to one another. As a result, analysis may provide a means to understand the operational bounds of these processing techniques.

B. Co-electrolysis Modeling Results

The co-electrolysis model was constructed to simulate the bench-scale co-electrolysis unit developed by O'Brien et al.[22] As a result, a significant amount of experimental data exists for model verification. In the first phase of the analysis, the open-cell potential was calculated as a function of reactor temperature. The open-cell potential is the operating voltage when the total ionic current is zero and provides an indication of how the rWGS reaction proceeds in the absence of the electrochemical reactions. These results are included in fig. 6.

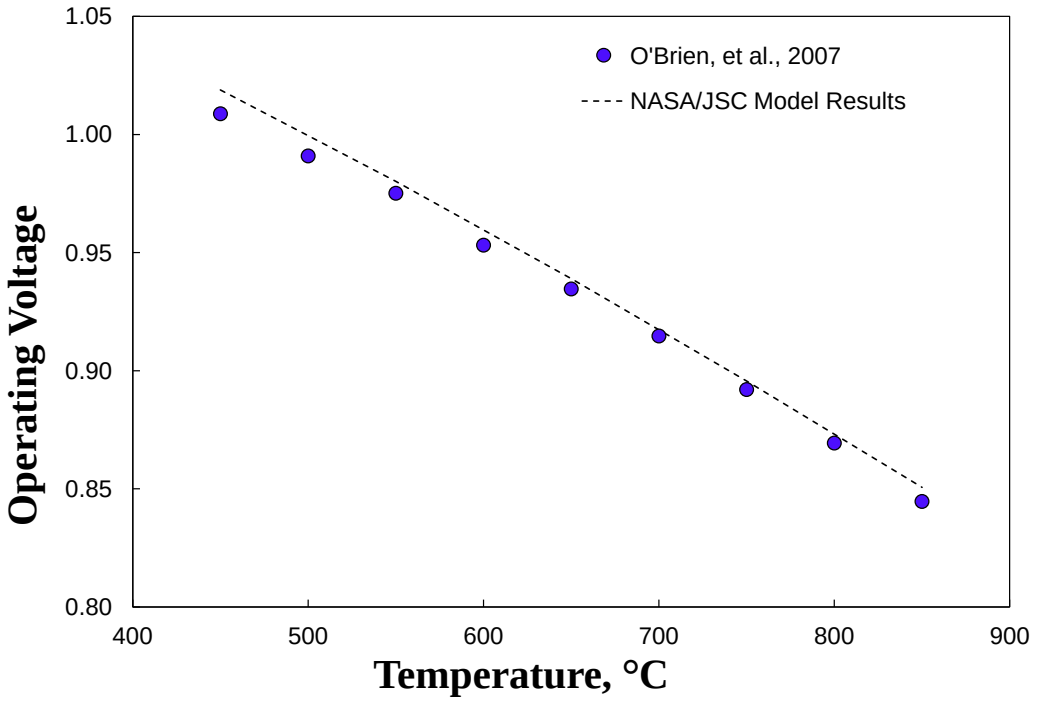

Figure 6: Open-cell operating voltage in comparison to results collected by O'Brien et al.[22] Component flow rates are 35 sccm N_2, 4 sccm H_2, and 8 sccm CO_2. The dew point of the incoming gas stream was 54.5°F.

As indicated in fig. 6, the predicted Nernst potentials are within good agreement with respect to the experimental results within the range of expected operating temperatures (*i.e.* 600-800°C or 1112-1472°F). This suggests that the approach to modeling the reactor kinetics for the rWGS reaction in particular are applicable for this system. Moreover, O'Brien et al. present a chemical equilibrium model that provides similar results. The equilibrium model applies an equilibrium coefficient (see: eq. 23) and an atomic species balance to predict the open-cell voltage and outlet composition. While this approach is valid for the bench-scale apparatus where flow rates and compositions are precisely set, it does not account for the dynamics associated with the reaction process.

Since the goal of this effort is to develop air revitalization sub-system models that can plug-and-play with other components in an air revitalization system where flow rates and compositions rapidly change, it is necessary to capture dynamics associated with the co-electrolysis process. As a result, a significant departure was made from the chemical equilibrium model employed in previous studies.[1,22–24]

The electrochemical reaction was incorporated into the model and verified following the confirmation of the open-cell operating voltage results demonstrated in fig. 6. The challenge to applying the electrochemical reaction is that the system of equations that need to be solved rely on knowledge about an external heating rate and/or outlet temperature. One approach is to assume the reaction cell is well insulated and to apply an adiabatic condition for external heating. The material and energy balance equations can then be solved after applying the adiabatic assumption. However, this requires a solution to a triple integral (eq. 54) with bounds that are unknown until the solution is generated. McKellar et al. accomplished this using the HYSYS® software package (Aspen Technology Inc., Burlington, MA). HYSYS® employs a sequential block solving algorithm where a model is solved block-by-block until convergence is attained. Within the electrolyzer block, a logical adjust block was employed to find the outlet temperature satisfying the energy balance. Conversely, Aspen Custom Modeler® converts the system of highly-coupled partial differential equations to a system of algebraic ordinary differential equations that are solved simultaneously employing advanced linear algebra techniques and numerical time integration. Aspen Custom Modeler® readily computes integrals so long as the bounds are defined prior to the calculation. For the co-electrolysis model, the integral bounds are not known *a priori*. To overcome this challenge, a three-dimensional 8-point Gaussian quadrature technique was applied to convert eq. 54 to a polynomial approximation. This approach allows for the generation of solutions to the dynamic co-electrolysis model.

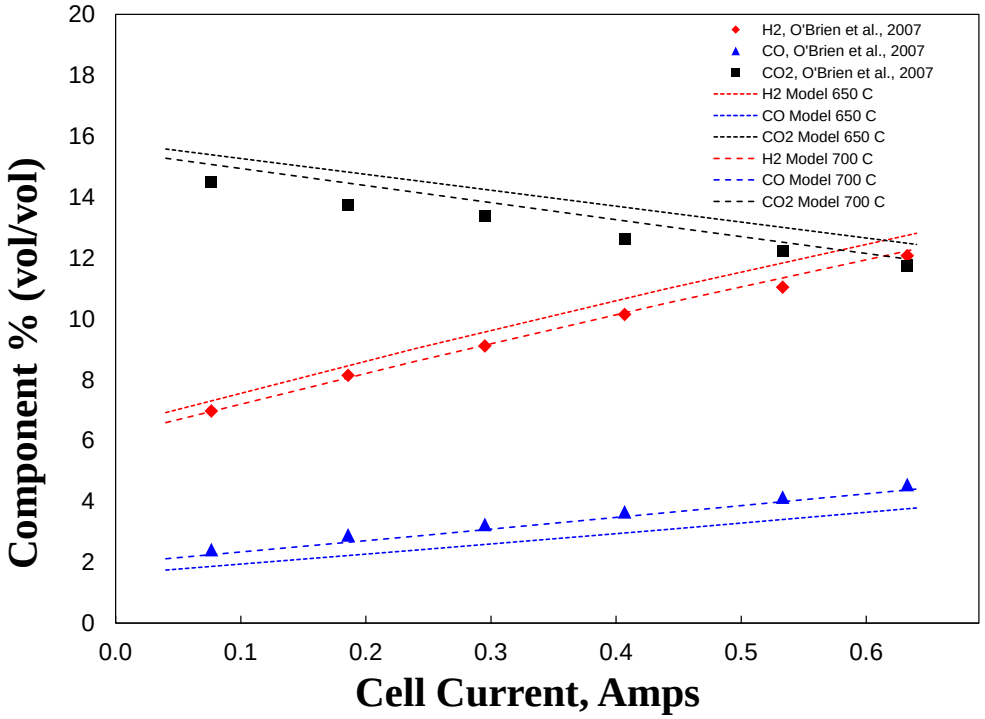

Figure 7: Outlet composition on a dry basis in comparison to results collected by O'Brien et al.[22]

O'Brien et al. verified their chemical equilibrium model against outlet gas compositions as a function of cell current ranging from 0.0 to 0.6 Amperes.[22] ASR values were experimentally determined based on a reference voltage. After exiting the reactor, the gas passes through a condensing heat exchanger to a gas chromatograph unit where composition was evaluated on a dry basis. Through this process, the gas cools and the precise reactor exit temperature is unknown by the time the gas is analyzed. Consequently, O'Brien et al. generated solutions to the chemical equilibrium model for a multitude of temperatures to determine what appears to be the appropriate exit temperature. Fig. 7 demonstrates outlet compositions for 650°C

and 700°C which are the temperatures summarized in by O'Brien et al. The outlet composition on a dry basis for the model shows good agreement with the experimental results. At temperatures lower than 650 °C (1202°F), the kinetics of the reaction become so slow that little to no change in composition is expected upon gas cooling. As a result, O'Brien et al. surmised the reactor outlet temperature is most likely around 700°C (1292°F). The agreement between the dynamic model developed at Johnson Space Center (JSC) and the experimental results of O'Brien et al. validate the model is reporting reasonable results.

The dynamic co-electrolysis model discussed herein provides a tool that can be integrated within larger system-level models for computer-aided design and optimization of future air revitalization for space exploration. Future work on this model will involve scaling the model from a single-cell to a multiple cell model with increased processing rates. To achieve scale-up, Arrhenius correlations for ASR as a function of temperature will need to be employed.[23]

IV. Conclusion and Future Work

To render missions beyond low-Earth orbit viable, mass of gas resources needs to be minimized. Regenerating useable resources from crew-expired gases is one approach to reducing launch mass. Carbon dioxide reduction is one approach to fulfilling these objectives. Currently, three processes are under investigation for CO_2 reduction during space exploration: (1) Sabatier reaction, (2) Bosch reaction, and (3) CO_2 and H_2O co-electrolysis. To date, a handful of bench-top and pilot-scale prototypes of these units have been built and evaluated. However, these prototypes were not necessarily built on a comparable scale for comparable processing rates. Moreover, the prototypes were not assessed for performance within the context of a larger air revitalization system where flow rates, pressure, temperatures, and inlet compositions are subject to rapid and dramatic perturbations. Consequently, there is an impetus toward creating first principles models to investigate performance of these techniques on a comparable scales with dynamic conditions. This report summarizes three first principles models created to fulfill this objective. At this point, the models exist; however, scales need to be altered and processing rates adjusted for a fair comparison between technologies. As a result, the model systems have yet to be integrated within a larger system. This report serves to explain the models as well as to present a year end status summary for the fiscal year 2011 efforts.

The Bosch model was constructed with an annular reactor geometry for the means of direct comparison to results reported elsewhere.[10,15] The Bosch model was deliberately constructed to maintain flexibility so that the Sabatier reaction can easily be incorporated within this model to fairly compare the reactor processes. The Bosch reactor system model has been developed and the pressure drop as a function of coke density has demonstrated good agreement with results reported elsewhere.[10,15] At this point, the numerical stability of the Bosch model could stand to be improved and is a short term goal for early fiscal year 2012.

The dynamic co-electrolysis model is a significant departure from the chemical equilibrium models for co-electrolysis reported elsewhere.[1,22–24] While both models report results within good agreement with one another and with experimental data, capturing the reactor dynamics is important for future system-level analytical investigations. The dynamic co-electrolysis model was compared against results for open-cell Nernst voltage as a function of temperature and outlet gas composition as a function of total ionic current.[22] In both cases, the model correlates well with the experimental data. The results from the model verification exercises provide confidence in the dynamic model. However, this relies on a model developed for a bench-scale counterpart. Consequently, scale-up needs to be performed for future efforts. To achieve scale-up, area specific resistance relationships versus temperature will need to be developed.

With respect to future work, the kinetic models rely on rate expressions that are very sensitive to the nature of the catalyst (*e.g.* catalyst material, shape, size dispersity, porosity, tortuosity). As catalysis for air revitalization is still under aggressive investigation,[25,26] these models will most likely require ongoing future updates.

V. Mathematical Model Nomenclature

A. Variables

A	Species list vector, [string variables]
A_c	Catalyst specific area or area of electrolysis cell, [m^2]
C_j	Concentration of component j, [kmol/m^3]
C_p	Constant pressure heat capacity of the gas-phase, [kJ/kmol-K]
F	Faraday's constant, [96.4853 $\times 10^3$ C/mol]
$\Delta G_{R,j}$	Gibbs energy of reaction for component j, [kJ/mol]
H,H_j	Mixture enthalpy or enthalpy of component j, [kJ/mol]
H_j^o	Standard state enthalpy of component j, [kJ/mol]
$\Delta H_{f,j}^o$	Standard state enthalpy of formation for component j, [kJ/mol]
K, K_i	Equilibrium coefficient for reaction i, [varies with reaction]
k, k_i	Reaction rate coefficient, [varies with reaction]
H	Enthalpy, [kJ/mol]
I_e	Total ionic density, [Amperes-m^2]
i_c	Cell current, [Amperes]
R_g	Universal gas constant, [8.314472 J/K-mol -or- Pa-m^3/mol-K]
$R_{i,j}$	Species reaction rate for species i and reaction j, [kmol/m^3-hr]
r	Radial coordinate, [m]
r_i	Reaction rate for reaction i, [kmol/m^3-hr]
M_j	Molecular weight of species j, [kg/kmol]
m_j	Mass density of species j, [kg/m^3]
N, N_j	Molar flow rate of component j, [kmol/s]
ΔN_O	Rate of monatomic oxygen removal, [kmol/s]
n_c	Number of electrolysis cells, [No.]
n_j	Moles of component j, [kmol]
P	Pressure, [bar]
Q	External heat transfer rate, [kW]
T	Temperature, [K]
T_r	Temperature of the reactor wall, [K]
t	Time, [hr]
V	Volume -or- reactor volume, [m^3]
$\dot{V}$	Volumetric flow rate, [m^3/hr]
V_{N}	Mean Nernst potential, [volts]
V_{op}	Operating potential, [volts]
$\vec{v}$	Velocity vector in three-space, [m/s]
v, v_r	Velocity in radial coordinate, [m/s]
W	Electrical work, [kW]
Z	Compressibility factor, [unitless]
z_j	Mole fraction of component j, [kmoles i/kmole]

B. Greek Letters

Δ	Change with respect to a variable
ϵ	Void fraction, [unitless]
ϵ_o	Void fraction prior to reaction representing the void fraction of the catalyst, [unitless]
η	Approach to equilibrium, [varies with reaction]

κ Darcy permeability, [m^2]

λ Temperature dependency parameters for equilibrium coefficient calculation

μ Viscosity, [Pa·s]

ν Stoichiometric coefficient matrix, [unitless]

ϕ_j Convective flux of component j, [kmol/m-s]

ρ Molar density of interstitial gas phase in a reactor, [$kmol/m^3$]

ρ_i Molar bulk density of component i, [$kmol/m^3$]

ξ Divisor in mean Nernst potential calculation

C. Superscripts & Subscripts

c Associated with catalyst or electrolysis cell variable

i Associated with a particular reaction listed in reaction rate vector r

j Associated a particular species listed in species list A

w Associated with a wall variable

References

[1]McKellar, M., Sohal, M., Stoots, C.M., M. L., Luna, B., and Abney, M., "Mathematical Analysis of High-Temperature Co-electrolysis of CO_2 and O_2 Production in a Closed-Loop Atmosphere Revitalization System," Tech. Rep. INL/EXT-10-19726, Idaho National Laboratory, Idaho Falls, ID, March 2010.

[2]Sridhar, K. and Iacomini, C., "Combined H_2O/CO_2 Solid Oxide Electrolysis for Mars In Situ Resource Utilization," *J. of Propulsion and Power*, Vol. 20, No. 5, 2004, pp. 892–901.

[3]Hwang, H., *A study of the application of membrane-based reactive separations to carbon dioxide methanation*, Ph.D. thesis, University of Southern California, Los Angeles, California, 2009.

[4]Lunde, P. and Kester, F., "Rates of methane formation from carbon dioxide and hydrogen over a ruthenium catalyst," *Journal of Catalysis*, Vol. 30, No. 3, 1973, pp. 423–429.

[5]Lunde, P. and Kester, F., "Carbon dioxide methanation on a ruthenium catalyst," *Industrial & Engineering Chemistry Process Design and Development*, Vol. 13, No. 1, 1974, pp. 27–33.

[6]Jeng, F., "Modeling and Analysis of Test Data of the Life Support System Integration Facility Carbon Dioxide Reduction Subsystem," Tech. Rep. MDS-1092, Lockheed Martin, Houston, TX, February 1995.

[7]Jeng, F., "Analyses of Integrated CDRA/Sabatier CRS EDU Test Data and Upgrade of the Integrated CDRA/Sabatier CRS Model in FY05," Tech. Rep. ESCG-4470-05-TEAN-DOC-0121, Engineering and Science Contract Group, Houston, TX, September 2005.

[8]Jeng, F., "Status of Analysis Support to the Integrated Sabatier EDU Test, Rev. A," Tech. Rep. MSAD-04-0286, Rev. A, Lockheed Martin Space Operations, Houston, TX, January 2005.

[9]Anderson, M., "Sabatier Reactor ACM Model Report," Tech. Rep. MSAD-02-0476, Lockheed Martin Space Operations, Houston, TX, September 2002.

[10]Bunnell, C., Boyda, R., and Lee, M., "Optimization of the Bosch CO_2 reduction process," *SAE International*, 1991.

[11]Stoots, C., "Production of synthesis gas by high-temperature electrolysis of H_2O and CO_2 (co-electrolysis)," Presentation: Columbia University, New York.

[12]Iacomini, C., "Demonstration of a stand-alone solid oxide electrolysis stack with embedded Sabatier reactors for 100% oxygen regeneration," *41st International Conference on Environmental Systems*, Am. Inst. Astronaut. & Aeronaut., Portland, OR, 2011, Paper No. 2011–5016.

[13]Rawlings, J. and Ekerdt, J., *Chemical reactor analysis and design fundamentals*, Nob Hill Publishing, Madison, WI, 2002.

[14]Fogler, H., *Elements of chemical reaction engineering*, Prentice-Hall Englewood Cliffs, NJ, 1992.

[15]Fritts, S., "Bosch Carbon Dioxide Reduction System Model," Tech. Rep. ESCG-4470-08-TEAN-DOC-0282, Engineering and Science Contract Group, Houston, TX, June 2008.

[16]Sandler, S., *Chemical and engineering thermodynamics*, John Wiley & Sons, 1989.

[17]Poling, B., Thomson, G., Friend, D., Rowley, R., and Wilding, W., *Perry's Chemical Engineer's Handbook*, chap. 2: Physical and Chemical Data, McGraw-Hill, 8th ed., 2008.

[18]Smith, B., Loganathan, M., and Shantha, M., "A Review of the Water Gas Shift Reaction Kinetics," *International Journal of Chemical Reactor Engineering*, Vol. 8, No. 4, 2010, pp. 1–32.

[19]Rotaru, P. and Blejoiu, S., "Kinetics and mechanism of CO_2 methanation on a nickel catalyst," *Journal of the Indian Chemical Society*, Vol. 78, No. 7, 2001, pp. 343–355.

[20]Snoeck, J., Froment, G., and Fowles, M., "Steam/CO_2 Reforming of Methane. Carbon Filament Formation by the Boudouard Reaction and Gasification by CO_2, by H_2, and by Steam: Kinetic Study," *Industrial Engineering & Chemical Research*, Vol. 41, 2002, pp. 4252–4265.

[21]SAIC, "Fuel Cell Handbook," *US and Department of Energy, Office of Fossil Energy, West Virginia, USA*, 2002.

[22]O'Brien, J., Stoots, C., Herring, J., and Hartvigsen, J., "High-Temperature Co-Electrolysis of Steam and Carbon Dioxide for Direct Production of Syngas; Equilibrium Model and Single-Cell Tests," Tech. Rep. INL/CON-07-12241, Idaho National Laboratory, Idaho Falls, ID, July 2007.

[23]McKellar, M., O'Brien, J., Stoots, C., and Hawkes, G., "Process Model for the Production of Syngas Via High Temperature Co-Electrolysis," Tech. Rep. INL/CON-07-12818, Idaho National Laboratory, Idaho Falls, ID, November 2007.

[24]McKellar, M., Sohal, M., Stoots, C.M., M. L., Luna, B., and Abney, M., "The Concept and Analytical Investigation of CO_2 and Steam Co-Electrolysis for Resource Utilization in Space Exploration," *41st International Conference on Environmental Systems*, Am. Inst. Astronaut. & Aeronaut., Barcelona, Spain, 2010, Paper No. 2010–6273.

[25]Abney, M. and Mansell, J., "The Bosch Process - Performance of a Developmental Reactor and Experimental Evaluation of Alternative Catalysts," *41st International Conference on Environmental Systems*, Am. Inst. Astronaut. & Aeronaut., Barcelona, Spain, 2010, AIAA 2010-6272.

[26]Abney, M. and Mansell, J., "Evaluation of Bosch-Based Systems Using Non-Traditional Catalysts at Reduced Temperatures," *41st International Conference on Environmental Systems*, Am. Inst. Astronaut. & Aeronaut., Portland, OR, 2011, AIAA 2011-5059.